Oxidation mechanism of $LaTiO_{3.5}$ thin films

J. W. Seo,[1,2] J. Fompeyrine,[2] H. Siegwart,[2] and J.-P. Locquet[2]
[1]*Institut de Physique, Université de Neuchâtel, CH-2000 Neuchâtel, Switzerland*
[2]*IBM Research, Zurich Research Laboratory, CH-8803 Rüschlikon, Switzerland*
(Received 31 October 2000; published 12 April 2001)

$LaTiO_{3.5}$ is a layered compound made up of four $LaTiO_3$ units: two regular perovskite units stacked between two distorted units that share an additional oxygen layer. In a single-crystalline thin film the (100) plane can be aligned parallel to the substrate surface, i.e., the additional oxygen layers are inserted parallel to the substrate surface. A detailed structural characterization reveals planar defects originating from substrate surface steps. These results, in combination with the *in situ* reflection high-energy electron-diffraction observations, suggest an oxidation mechanism using such antiphase boundaries as oxidation paths.

DOI: 10.1103/PhysRevB.63.205401 PACS number(s): 68.55.Ln, 77.84.Dy

I. INTRODUCTION

In perovskite-type compounds ABO_3, the transition element B can take a mixed valency depending upon oxygen or A-site doping, and many interesting properties can be obtained, e.g., high-T_c,[1] colossal magnetoresistive,[2,3] or ferroelectric compounds.[4] The perovskite $LaTiO_3$ compound allows a very rich and flexible chemistry: for instance, the oxygen content can be changed from 3.0 to 3.5, and the formal titanium valency varies between +III and +IV. The physical phase diagram of $LaTiO_{3+x}$ was studied extensively.[5,6] Starting with $x=0$, $LaTiO_{3+x}$ is semiconducting and becomes metallic with increasing oxygen content. For $x>0.2$ the additional oxygen (O_A) atoms order on infinite {110} perovskite planes, and form a semiconducting layered structure for $x=0.4$. For $x=0.5$, all the oxygen atoms order with a periodic stacking of these planes every 12.8 Å with four perovskite blocks (PB's) in between.[7] The $LaTiO_{3.5}$ compound—also called the ''2-2-7'' phase because of the stoichiometry—with monoclinic space group $P2_1$ is a very robust ferroelectric phase, with a critical temperature of $T_c=1773$ K,[8] a saturation polarization of 5 $\mu C/cm^2$, and a coercive field of 45 kV/cm. It has a unique polarization axis, which is the b axis in the monoclinic unit cell.

Although the physical and structural properties of $LaTiO_{3+x}$ are known in detail,[5,6] the oxidation mechanism during the transition from $x=0$ to 0.5 is not yet understood. Galy and Carpy[9] proposed a model for the oxygen-diffusion process in which the O_A planes migrate inside the ABO_{3+x} crystal. This model strongly focused on the migration process, and the question concerning the oxidation mechanism itself remained open.

Recently, we reported $LaTiO_{3.5}$ thin films successfully grown on $SrTiO_3$ (STO) and $LaAlO_3$ substrates.[10,11] In this paper, we report on a microstructural investigation of the $LaTiO_{3.5}$ thin film grown on (110)-oriented STO, and show that the oxidation mechanism is determined by antiphase boundaries (APB's), which act as oxygen-diffusion paths. This work aims to elucidate general concepts such as the oxidation process in perovskites, and the formation of long-range ordered structures.

II. EXPERIMENTAL DETAILS

Epitaxial thin films of $LaTiO_{3.5}$ are prepared in a molecular-beam-epitaxy system, using the block-by-block deposition method.[12] They are grown at 800 ± 10 °C on (110)-oriented STO substrates under a flow of atomic oxygen produced by a rf plasma source. This substrate orientation is the only one that allows epitaxial growth of single-crystalline $LaTiO_{3.5}$. Lanthanum and titanium are evaporated from an electron beam (e beam), and a deposition sequence of one La-O_x monolayer followed by one Ti-O_x monolayer is used. The oxygen background pressure is about 1.5×10^{-5} Torr before deposition, and decreases to 3×10^{-6} Torr with the (La,Ti) evaporation rates. After growth, the films are cooled under atomic oxygen at a rate of 10 °C/min. The structural quality of these films is monitored *in situ* by reflection high-energy electron diffraction (RHEED), and *ex situ* by x-ray diffraction (XRD) on a Siemens D500 diffractometer equipped with a graphite back monochromator. For the transmission electron microscopy (TEM) study, plan-view and cross-section samples were prepared by cutting, grinding, and finally thinning with an Ar-ion beam to electron transparency. High-resolution TEM (HRTEM) studies were performed with a JEOL 4000EX microscope (point-to-point resolution of 1.7 Å) and a JEOL 4000FX microscope operating at 400 kV, whereas conventional TEM was carried out with 200-kV microscopes, JEOL 2010. Simulated TEM images were calculated using the EMS Stadelmann software package.[13]

III. RESULTS

A. Epitaxial growth

Selected structural properties of the $LaTiO_{3.5}$ thin films grown on (110) $SrTiO_3$ were reported in Refs. 10 and 11. To summarize, the XRD diagram of the thin film revealed a homogeneous growth with an out-of-plane lattice spacing $d_\perp=1.2844\pm0.0005$ nm, which is very close to the reported (100) spacing of the $LaTiO_{3.5}$ unit cell in bulk phase ($d_{(100)}=1.2864$ nm). At low 2θ angles, finite-size oscillations were observed around the film diffraction peaks, which confirm that the roughness is not greater than ±1 unit cell.

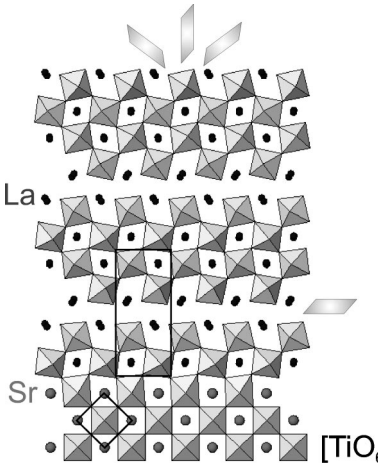

FIG. 1. Schematic drawing of the epitaxial relationship between (110) STO and (100)-oriented $LaTiO_{3.5}$ illustrated in projection onto the (a,b) plane of $LaTiO_{3.5}$. Filled circles indicate La and Sr atoms, and Ti atoms occupy the center of the $[TiO_6]$ octahedra. The respective unit cells are outlined by bold lines. The four equivalent {110} perovskite planes for oxygen insertion are indicated. The three planes on top suppress the lattice registry, whereas the obtained incorporation parallel to the interface does not affect the in-plane lattice mismatch.

In that case, the total film thickness was estimated to 12.5 ± 1 nm, i.e., about ten unit cells.

TEM studies were carried out along three orthogonal directions, i.e., one plan view and two cross-sectional views. From selected area electron diffraction (SAED), the (100) planes of the $LaTiO_{3.5}$ unit cell are confirmed to be parallel to the substrate surface. In addition, a monoclinic angle of 99° is observed, and the lattice parameters are derived as **a** $=13.0$ Å, **b**$=5.52$ Å, and **c**$=7.8$ Å. Accordingly, the epitaxial relationship between the film and the substrate is as follows (Fig. 1):

$$[110]_{STO} \| [010]_{227} \quad \text{and} \quad [001]_{STO} \| [001]_{227}.$$

During growth the in-plane lattice parameters are measured using RHEED. In Fig. 2(a) a typical RHEED pattern observed along the $[\bar{1}10]$ azimuth is shown, yielding well-

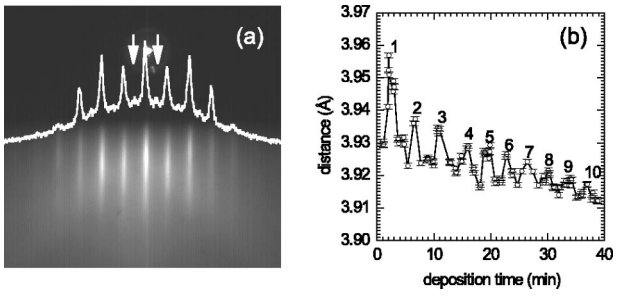

FIG. 2. (a) RHEED pattern observed along the $[\bar{1}10]$ azimuth during growth. A line scan illustrates the intensity modulation, and the arrows indicate the weak superstructure originating from the *c* axis obtained by doubling the perovskite unit. (b) Oscillation of the in-plane lattice parameter derived from RHEED.

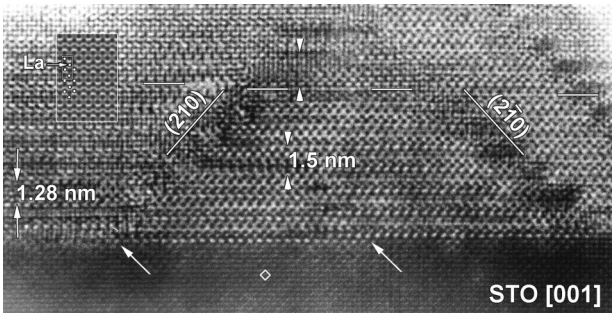

FIG. 3. [001] cross-section HRTEM image including a simulated image as an inset. APB's are present, with habit planes parallel to (211) and $(2\bar{1}1)$ planes, which appear in this image as projections (210) and $(2\bar{1}0)$. They originate from substrate steps (indicated by arrows) that give rise to a relative lattice displacement given by the step height. Owing to the inclined angle of 49° when two APB's meet, they annihilate each other at a thickness of about 15 nm.

defined streaks. A very weak twofold superstructure is seen, which can be confirmed by means of an intensity line scan drawn over the RHEED image. The positions of the superstructure, indicated by arrows, are in agreement with a *c* axis that is twice a perovskite unit. Figure 2(b) presents a variation of the in-plane lattice parameter derived from a series of RHEED patterns taken during an entire growth process. As the superstructure was not taken into account, the distance shown in the diagram corresponds to the *c*/2 axis parameter. However, the lattice parameter oscillates as a function of the deposition time, and the number of maxima is equal to the number of deposited unit cells. Therefore, the oscillation can be correlated directly with the formation of each $LaTiO_{3.5}$ unit cell. Besides the oscillations the distance decreases in general with increasing film thickness, starting at 3.93 Å. This value is given by the in-plane lattice parameter of STO at 800 °C because the film grows coherently with the substrate lattice in such an initial state. Indeed, the (100) lattice spacing of STO calculated using the thermal expansion coefficient ($\alpha \simeq 8.5 \times 10^{-6}$/K) (Ref. 14) is equal to 3.937 Å, which is in agreement with the value we observed. The subsequent decrease of the lattice spacing is associated with the strain relaxation in the film, and converges to a final value of about 3.91 Å, which fits well with half of the *c* axis. However, the unit-cell volume of $LaTiO_{3+x}$ basically decreases with increasing oxygen content.[5] In particular, for the *c* axis one finds bulk values of $c=7.92$ and 7.8 Å for $x=0$ and 0.5, respectively, which means that the final $LaTiO_{3.5}$ structure is obtained at the end of each oscillation. Hence the oscillation suggests the formation of four blocks of three-dimensional $LaTiO_{3+x}$ with a low oxygen content of $x < 0.2$ in the initial growth, and the subsequent transition to the $LaTiO_{3.5}$ phase.

In Fig. 3 a cross-sectional HRTEM image is shown, taken with the electron beam parallel to the $[001]_{STO}$ ($[001]_{227}$) direction. The film reveals a characteristic contrast consisting of bright and dark lines aligned parallel to the interface; their periodic distance averages to 12.8 Å, corresponding to the (100) interplanar spacing of the $LaTiO_{3.5}$ phase. Image simu-

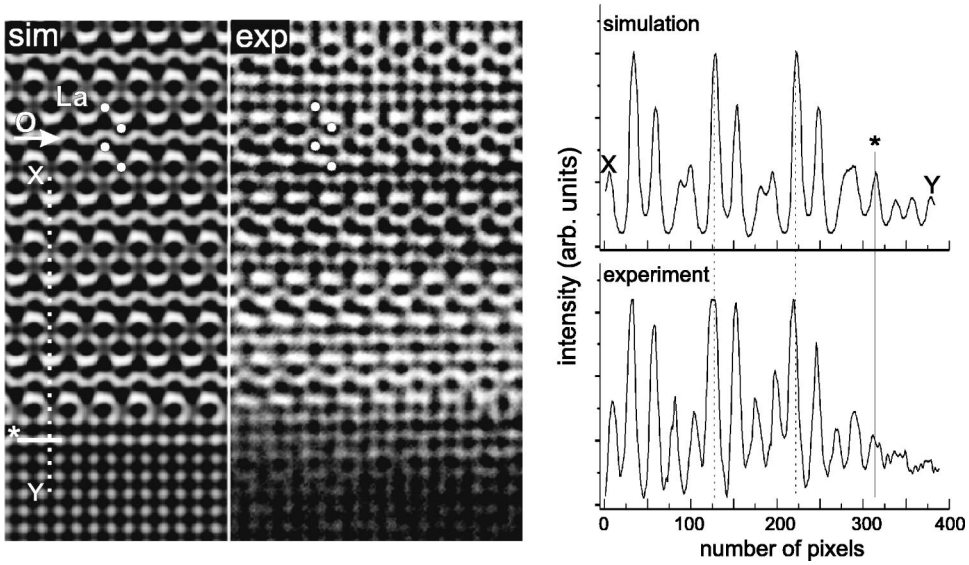

FIG. 4. Simulated and HRTEM images of the interface viewed along the [001] direction. The O_A plane gives rise to the wavy bright contrast indicated by an arrow. A line scan across the interface between points *X* and *Y* shows good agreement between these two images. The location of the interface is indicated by an asterisk. Accordingly, the first oxygen plane is inserted after two PB's at the interface.

lations were carried out to interpret the HRTEM image contrast properly. A reasonable fit with the experimental image contrast is obtained, assuming a sample thickness of 6 nm and a defocus value of -60 nm (see the inset of Fig. 3). Accordingly, the additional oxygen plane gives rise to the characteristic bright (100) lattice fringes. Such (100) lattice fringes are observed in the film throughout the entire image, pointing out the homogeneous (100) orientation of the film. The homogeneity is frequently disturbed by the presence of APB's, which are observed in all three viewing directions (see Sec. III C).

B. Interface structure

The interface is atomically flat and contains no amorphous or secondary phase layers. Image simulations have been performed to determine the stacking sequence of the interface. Different arrangements for the interface are considered, depending on the location of the additionally inserted oxygen plane. As the surface layer of (110)-oriented $SrTiO_3$ consists of rows of Sr and Ti sites, the Sr sites are assumed to be replaced by La in $LaTiO_3$. The best agreement was obtained when the O_A plane is inserted after two blocks of perovskite. Figure 4 shows the calculated and experimental images of the interface. The O_A plane correlates with the wavy line contrast, indicated by an arrow between two adjacent La atoms. At the interface, strongly pronounced bright and dark dots are seen, whereas the wavy line typical for the additional oxygen plane is missing. The location of the interface can be additionally confirmed by the line scan across the interface along the [100] direction between the positions *X* and *Y* as shown in Fig. 5. The intensity variation observed in both images is in good agreement. In the (010) orientation, the interface stacking sequence has been determined in the same manner, i.e., by comparing it with simulations and taking intensity profiles. The result obtained was once again in good agreement, confirming that the first O_A layer is incor-

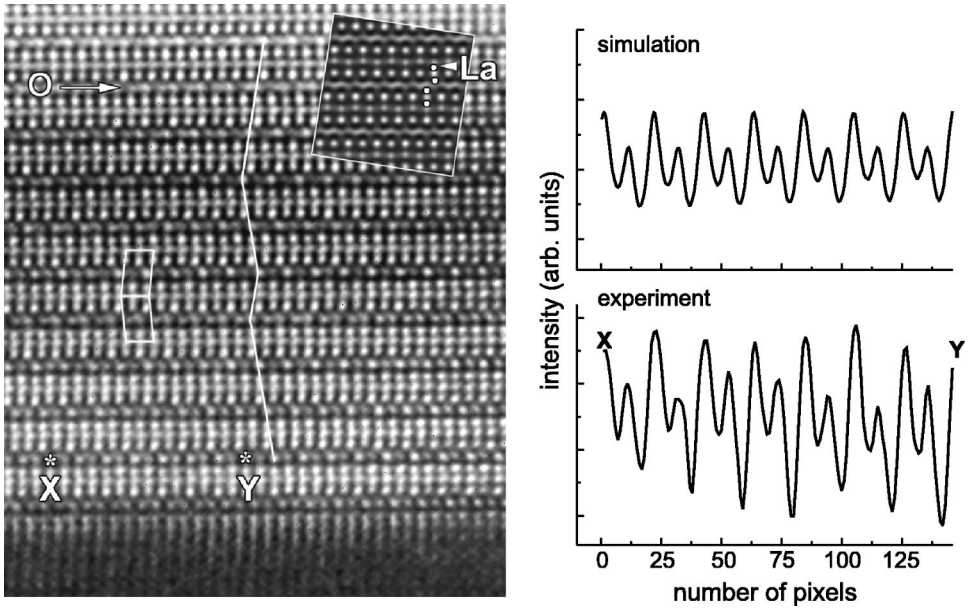

FIG. 5. An enlarged HRTEM image of ''2-2-7'' in the (010) orientation. The doubling of the unit cell along the *c* axis can be recognized by the variation of the intensities of bright dots, e.g., between the sites marked *X* and *Y*. The intensity profile confirms the variation in the HRTEM image as well as that of the simulated image in the inset. The presence of twins is proved by the change of the maximum peak positions determined by the line scan of each layer, as indicated by the white line.

porated after two PB's. Consequently, the stacking sequence at the interface is two blocks/oxygen layer/four blocks/ oxygen layer/four blocks, and so on. Such a stacking sequence is observed consistently everywhere at the interface, and also at interface regions adjacent to an APB. Intuitively, this seems inconsistent with the RHEED results, which indicate that the $LaTiO_{3.5}$ unit is only formed after four PB's (see Sec. III A). This will be explained in Sec. IV.

C. Defect structure

Antiphase boundaries are the most predominant defects, as can be seen in Fig. 3. Their occurrence is rather irregular, and the spacing varies from a few nanometers up to 100 nm. The estimated average value is 30 nm. The contrast in the defect region is rather broad, indicating that the habit planes are inclined in this projection. In Fig. 3 the intersection between APB's and the (001) plane is seen parallel to [120] and $[1\bar{2}0]$ directions. Indeed, in a $[1\bar{1}0]_{STO}$ image, APB's were found parallel to [102] and $[10\bar{2}]$ directions, whereas in a plan view their traces are parallel to [011] and $[0\bar{1}1]$. Consequently, the habit planes are determined to be the (211) and $(2\bar{1}1)$ planes.

The APB's originate from substrate surface steps, as can be seen in the interface region indicated by arrows in Fig. 3. Here these steps yield a height of $d_{(110)}$, which gives rise to a displacement of 2.76 Å in the film. Nevertheless, occasional $2\times d_{(110)}$ or $3\times d_{(110)}$ steps also exist. In the film they lead to a lattice displacement of 5.52 or 8.28 Å, respectively. The defects can extend throughout the entire film thickness. Owing to an angle of about 49° given by the habit plane and the interface plane, two APB's frequently meet and annihilate each other. Stacking faults parallel to the substrate are occasionally found between such APB's. These defects translate into a shift of the O_A layer from one in every four PB's to one in every five PB's, leading to an interplanar spacing perpendicular to the interface of about 1.5 nm. The measured value corresponds to the projected *a* axis of the $La_5Ti_5O_{17}$ phase.[7]

D. Twin structure

A twinned fragment of $LaTiO_{3.5}$ phase has been observed in the $[010]_{227}$ view. The superreflections in the SAED pattern, which are in agreement with the superstructure seen by RHEED (Fig. 2), are faint and barely visible in reproductions. Figure 5 shows an enlargement of the [010] HRTEM image. A slight intensity modulation of the bright dots, aligned parallel to the interface, indicates a doubling of the basic perovskite unit cell compared to the true unit cell with $c=7.8$ Å. The intensity profile, measured for instance between the positions marked by *X* and *Y*, clearly shows the contrast modulation. Such an intensity variation is also present in the equivalent line scan of a calculated image in Fig. 5(b).

By connecting the bright dots between subsequent $LaTiO_{3.5}$ units, an angle of 98° or 82° can be derived, which corresponds to the monoclinic angle of the unit cell or to its supplementary angle. In Fig. 5 all four units next to the interface can be connected with the 98° angle, whereas the angle abruptly changes to $180°-98°=82°$, indicating that the next layer is the other twin variant. In the HRTEM image the twin configuration is estimated and outlined using the position of maximum intensity in the line scan. For clarity, the unit meshes for twins I and II are indicated separately. This structure can be explained by the presence of twin boundaries parallel to the substrate surface. The twinning symmetry operation is given by a 180° rotation around the *c* axis, and not by a mirror operation. The sequence of the twin variants seems to be rather irregular; in the presented image the variant with an inclined angle of 98° dominates. Within each layer, only one twin variant is observed, i.e., the angle does not change from 98° to 82° unless the layer is interrupted by an APB.

IV. DISCUSSION

The growth procedure of a $LaTiO_{3.5}$ thin film is mainly determined by two parameters: (i) lattice mismatch, and (ii) the oxidation process. STO is a perfect substrate for the growth of low-oxygen-phase $LaTiO_3$ because of its perovskite structure and the small lattice mismatch (approximately 1.3%). For the growth of the layered compound $LaTiO_{3.5}$ the oxygen insertion is restricted because any insertion leads to an increase of the lattice parameter perpendicular to the inserted plane. Moreover, oxygen incorporation leads to the monoclinic unit cell and to the relative lattice displacement of about 1/4[001] between the PB's separated by the oxygen plane. Therefore, no coincident sites can be obtained on STO unless the O_A insertion takes place parallel to the substrate surface and the in-plane lattice mismatch is not strongly affected. On a (110)-oriented STO substrate, such incorporation can be obtained. This corresponds to the (100)-oriented growth of $LaTiO_{3.5}$ which has been observed in our study. The lattice mismatch is small: -0.47% and 0.12% for the *b* and *c* axes, respectively. On the other hand, with respect to the oxidation process, the (100) orientation is not favorable compared to other variants, because the oxygen plane is not directly connected to the surface where a high atomic oxygen flow is present.

The main question to be answered is how the oxidation proceeds in detail. To answer this question we have to consider the top and bottom parts of the film separately. As we reported previously,[15] the (100)-oriented growth is obtained for the initial growth of the thickness up to approximately 15 nm, whereas the film exceeding this critical value reveals a three-dimensional perovskite structure with some intergrowth of the layered phase, indicating that the oxygen content is low, $x<0.2$. As the epitaxial constraint determined by the substrate does not change significantly during growth, we have to conclude that it is the oxidation process itself that changes for a thickness $d>15$ nm. The main difference between the film below and above 15 nm is the presence of APB's. As observed in Fig. 3, APB's occur with habit planes parallel to (211) and $(2\bar{1}1)$, yielding an inclined angle of 49° with respect to the substrate surface. The HRTEM results indicate that APB's originate from substrate surface steps (see Fig. 3), with an average spacing of 30 nm. Taking

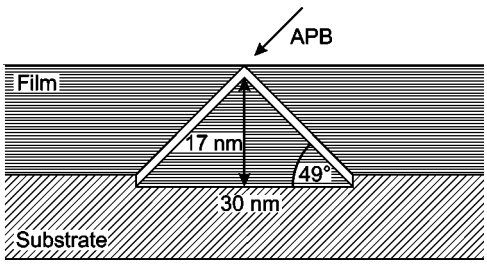

FIG. 6. Schematic drawing of two APB's originating from substrate surface steps with a spacing of about 30 nm. Taking the (211) and $(2\bar{1}\bar{1})$ habit planes into account, the film thickness where the APB's merge can be calculated to be 17 nm.

the angle and the spacing between two steps, a simple calculation can be made—illustrated in Fig. 6—which suggests that APB's merge at a film thickness of 17 nm. When two APB's meet, they can annihilate each other when the sum of the displacement vectors is equal to a lattice vector of $LaTiO_{3.5}$, or they can combine to one single APB with a new resulting displacement vector. In any case the density of APB's decreases drastically and exceeds 17 nm, which is in perfect agreement with the 15 nm observed. Moreover, the observed habit planes of APB's—(211) and $(2\bar{1}\bar{1})$—correspond to two equivalent {110} perovskite planes, which are the O_A insertion planes in this layered compound. Hence our observations strongly suggest that APB's act as oxygen diffusion channels.

The influence of extended defects on the reactivity of solids was pointed out by other authors.[16–19] Direct intercalation of oxygen into planar defects was observed by Arrouy *et al.*[18] in the La_2CuO_4 system. Using electrochemical oxidation, they showed that planar defects enable the oxygen transport into the film, followed by a slower oxygen diffusion into the interstitial sites along the in-plane directions. The diffusion coefficients can normally be 6–8 orders of magnitude higher in such planar defects than in the bulk material.[19] For the $LaTiO_{3.5}$ system the difference might be smaller, because both planes correspond to equivalent {110} perovskite planes for oxygen incorporation.

As shown in Fig. 3, APB's originate from substrate surface steps. Such surface inhomogeneities lead to a local distortion of the film lattice on top, where the consideration of the ideal two-dimensional lattice mismatch, as mentioned at the beginning of the discussion, is no longer valid. O_A can easily be inserted at such distorted locations along (211) or $(2\bar{1}\bar{1})$ planes, and oxygen channels are created. Subsequent in-plane oxidation starts to form an entire O_A plane parallel to the interface. This explains why layers below 15 nm show a homogeneous *a*-axis growth, while, for $d>15$ nm, when only few APB's are available, the oxygen insertion process is hindered and the film cannot be fully oxidized. Without oxygen channels the insertion can still partly occur, owing to the high atomic-oxygen pressure in the growth chamber, leading to the $LaTiO_{3.5}$ intergrowths observed in three-dimensional perovskite units.[15]

In order to make a numerical estimate, we can calculate the diffusion coefficient (D) using the diffusion relation[20]

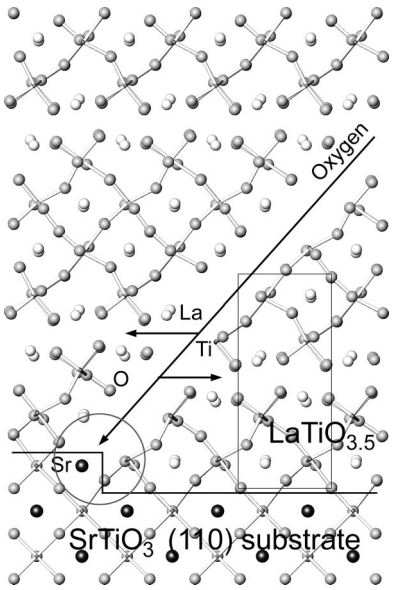

FIG. 7. Schematic drawing of the oxidation procedure. At a substrate surface step an APB is created because of local distortion. The oxidation takes place first along the habit plane of the APB's, which corresponds to a typical oxidation (110) perovskite plane. Subsequently, oxidation parallel to the (100) plane occurs, resulting in valency change from Ti^{+3} to Ti^{+4}. Hence the presence of these faults is a necessary condition for efficient oxidation.

$d_f=\sqrt{(Dt)}$, where d_f corresponds to the maximum width of the sample that oxides laterally. This can be estimated by the average distance of the APB's for $d>15$ nm: assuming that alternating pairs of APB's merge and hence annihilate each other, the average APB distance is approximately 120 nm. This might be an estimate of the critical size for lateral oxidation. With a time t of about 100 s necessary to oxidize, which corresponds to the time necessary to grow one layer of $LaTiO_{3.5}$, the in-plane diffusion coefficient can be calculated to be approximately 10^{-12} cm^2/s. In contrast, the diffusion coefficient without oxidation channels can be estimated to be 10^{-15} cm^2/s using the same diffusion time and the typical width ($d_f=20$ nm) of $LaTiO_{3.5}$ intergrowths observed.[15] This clearly illustrates the necessity of planar defect for the oxidation process.

To summarize, we propose an oxidation mechanism based on three steps, which is shown schematically in Fig. 7: (i) nucleation of APB's at substrate surface steps, (ii) O_A insertion in (211) [or $(2\bar{1}\bar{1})$] planes along APB's, and (iii) O_A insertion in $(100)_{227}$ plane. Based on our oxidation model, three possible ways to form $LaTiO_{3.5}$ can be considered: the ''2-2-7'' unit is formed (i) directly from the beginning of the growth process, (ii) by the transition of the three-dimensional perovskite to the fully oxidized compound during the growth of one PB unit after the other, or (iii) after the entire growth process upon cooling. Our RHEED observations[10] (see Fig. 2) strongly suggest the second possibility. The ordering of oxygen atoms and the formation of the true $LaTiO_{3.5}$ structure within one unit cell occurs when four PB's have been deposited. This contrasts with the two PB's found at the

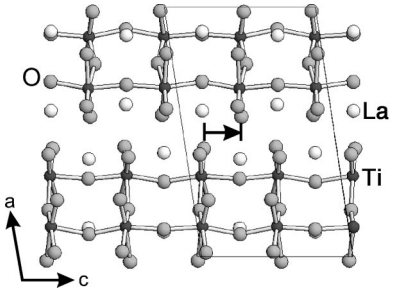

FIG. 8. Schematic projection of the ''2-2-7'' structure along the [010] direction. The unit cell is outlined. The O_A yields a relative displacement of bottom and top PB of about 1/4[001].

interface by HRTEM (Fig. 4), but these two results become consistent when $LaTiO_{3.5}$ is assumed to form by a phase transition from four PB's of $LaTiO_3$ (as observed by RHEED) to the $LaTiO_{3.5}$ structure, introducing the O_A layer between two blocks. The latter corresponds to the final oxidation state observed by HRTEM.

The insertion of O_A is not simply an intercalation of oxygen atoms; forming this structure requires a displacement of the two top PB's relative to the two bottom PB's by approximately 1/4[001] (see Fig. 8). This process cannot be done in a random way—this would lead to huge strains in adjacent unit cells—and as a consequence it takes place when the top two PB's can be ''lifted off'' coherently and shifted along $\pm 1/4[001]$. The presence of APB's would help such coherent ''lift off'' because APB's divide the film into small coherent regions. But why does O_A occur after two PB's, not after three? This must be related to the charge transfer. In the $LaTiO_{3.5}$ compound, the overall valency is Ti^{+IV}, but the local oxygen arrangements around Ti suggest a sequence of Ti^{+III} and Ti^{+V}. To be more precise, Ti atoms in the perovskite block are adjacent to six edge-sharing oxygen atoms, whereas the Ti atoms adjacent to O_A are surrounded by four edge-sharing and two ''free'' octahedra-corner oxygen atoms, leading to a local valency of Ti^{+III} and Ti^{+V}, respectively. The latter does not exist and is therefore always compensated for by charge transfer from the former. Inserting O_A after two or three PB's would result in successive local valence sequences of (i) +III−+V−+V−+III or (ii) +III−+III−+V −+V. Besides Ti^{+V} becoming unstable at the surface, in the latter case, charge neutrality would require charge transfer over 2–3 neighboring unit cells compared to the former case, where transfer to the nearest neighbor is sufficient. A more correct physical picture can be obtained by considering the bond valence sum[21] $V_i = \Sigma_j \exp[(R_{ij} - d_{ij})/b]$, where d_{ij} is the bond length between two atoms i and j. The term b is a constant, where $b = 0.37$ Å. In our case, the bond-valence parameters R_{ij} of Ti-O bonds were set equal to 1.791 and 1.815 for Ti^{+III} and Ti^{+IV}, respectively.[21] In $LaTiO_{3.5}$, the Ti atoms in the regular PB's yield $V_i = 3.76$, which is significantly higher than $V_i = 3.0$ in $LaTiO_3$. In contrast, the Ti atoms adjacent to O_A lead to $V_i = 4.16$. Hence, in total, the valence sums average to 3.96, in agreement with 4.0 of the expected Ti^{+IV}. This calculation clearly illustrates the local variation of the Ti valence and the strong charge transfer between the two Ti atoms. Such charge transfer might be essential for charge compensation and for the stability of the layered compounds.

The last question to address is whether our thin film is ferroelectric like the bulk phase. Twin structure has been observed in $LaTiO_{3.5}$ bulk structure[22] as well as in our thin films (see Sec. III D). In the $LaTiO_{3.5}$ system the presence of twins is a direct indication of a noncentrosymmetric unit cell, therefore, such twins can occur because of dipole-dipole interaction between each unit cell layer. Hence it is an indication of domains with spontaneous polarization in this system, and suggests ferroelectricity in our thin film.[23] This topic will be discussed in detail more in a forthcoming paper.

V. CONCLUSION

We have grown epitaxial (100)-oriented $LaTiO_{3.5}$ thin films on (110) $SrTiO_3$, for which the additional oxygen (O_A) plane is parallel to the interface. Oxygen diffusion occurs first along antiphase boundaries, which are used as oxidation channels. The growth mechanism of these films is not driven by the direct formation of the $LaTiO_{3.5}$ structure from the beginning, but by the formation of perovskite blocks and by the subsequent oxygen insertion into the final $LaTiO_{3.5}$ structure. This is probably due to the stacking of Ti atoms with different valencies.

ACKNOWLEDGMENTS

We especially acknowledge J. G. Bednorz for stimulating discussions and encouragement. We thank O. Becker, Ø. Fischer, S. Gariglio, P. Martinoli, A. Reller, and J.-M. Triscone for fruitful discussions. We are also very grateful to the Institut für Festkörperforschung (Forschungszentrum Jülich) for provision of TEM facilities. This work was supported by the Swiss National Science Foundation 2129-42367.94 as well as the Swiss Priority Project ''Minast.''

[1] J. G. Bednorz and K. A. Müller, Z. Phys. B: Condens. Matter **64**, 189 (1986).
[2] K. Chahara, T. Ohno, M. Kasai, Y. Kanke, and Y. Kozono, Appl. Phys. Lett. **62**, 7 (1993).
[3] R. von Helmolt, J. Wecker, B. Holzapfel, L. Schulz, and K. Samwer, Phys. Rev. Lett. **71**, 2331 (1993).
[4] F. Jona and G. Shirane, *Ferroelectric Crystals* (Pergamon Press, Oxford, 1962).
[5] F. Lichtenberg, D. Widmer, J. G. Bednorz, T. Williams, and A. Reller, Z. Phys. B: Condens. Matter **82**, 211 (1991).
[6] T. Williams, F. Lichtenberg, D. Widmer, J. G. Bednorz, and A. Reller, J. Solid State Chem. **103**, 375 (1993).
[7] T. Williams, H. Schmalle, A. Reller, F. Lichtenberg, D. Widmer, and J. G. Bednorz, J. Solid State Chem. **93**, 534 (1991).
[8] S. Nanamatsu, M. Kimura, K. Doi, S. Matsushita, and N. Yamada, Ferroelectrics **8**, 511 (1974).

[9] J. Galy and A. Carpy, Philos. Mag. **29**, 1207 (1974).
[10] J. Fompeyrine, J. W. Seo, and J.-P. Locquet, J. Eur. Ceram. Soc. **19**, 1493 (1999).
[11] J. W. Seo, J. Fompeyrine, and J.-P. Locquet, in *Superconducting and Related Oxides: Physics and Nanoengineering III*, edited by D. Pavuna and I. Bozovic [Proc. SPIE **3481**, 326 (1998)].
[12] J.-P. Locquet and E. Mächler, MRS Bull. **19**, 39 (1994).
[13] P. A. Stadelmann, Ultramicroscopy **21**, 131 (1987).
[14] H. J. Scheel, MRS Bull. **19**, 26 (1994).
[15] J. W. Seo, J. Fompeyrine, and J.-P. Locquet, in *Electron Microscopy* (Institute of Physics Publishing, Bristol, 1998), Vol. II, pp. 351 and 352.
[16] J. Galy, Acta Crystallogr., Sect. B: Struct. Sci. **48**, 777 (1992).
[17] G. Van Tendeloo and S. Amelinckx, Physica C **176**, 575 (1991).
[18] F. Arrouy, J.-P. Locquet, E. J. Williams, E. Mächler, R. Berger, Ch. Gerber, C. Monroux, J.-C. Grenier, and A. Wattiaux, Phys. Rev. B **54**, 7512 (1996).
[19] E. Goldberg, A. Nemudry, V. Boldyrev, and R. Schöllhorn, Solid State Commun. **110**, 223 (1998).
[20] L. A. Girifalco, *Atomic Migration in Crystals* (Blaisdell, New York, 1964).
[21] N. E. Brese and M. O'Keeffe, Acta Crystallogr., Sect. B: Struct. Sci. **47**, 192 (1991).
[22] H. Schmalle, T. Williams, A. Reller, A. Linden, and J. G. Bednorz, Acta Crystallogr., Sect. B: Struct. Sci. **49**, 235 (1993).
[23] J. W. Seo, J. Fompeyrine, H. Siegwart, and J.-P. Locquet, in *Proceedings of the 12th European Congress on Electron Microscopy*, edited by J. Gemperlová and I. Vávra (Czechoslovak Society for Electron Microscopy, Brno, 2000), Vol. II, pp. 191 and 192.